ADVANCED FUNCTIONAL MATERIALS
www.afm-journal.de

Stomata-Inspired Membrane Produced Through Photopolymerization Patterning

*Hyejeong Kim and Sang Joon Lee**

The programmed movements of responsive functional hydrogels have received much attention because of their abundant functions and wide range of engineering applications. In this study, an innovative stomata-inspired membrane (SIM) is fabricated by using a temperature-responsive hydrogel through a simple, cost-effective, and high-throughput patterned photopolymerization. Polymerization-induced diffusion on the macroscale surface results in formation of a double-parted polymer membrane with fine pores after single illumination. After heating the SIM, the less deformable thick frame supports the whole structure and the highly deformable thin base regulates pore shape. Among various SIM types, the slit pores of monocot SIM, which are lined up in parallel, exhibit the largest radius deformation. The morphological configuration of the SIM can be easily controlled by changing the photomask for a given application. As the developed SIM features the sensing-to-activation functions of stimuli-responsive hydrogels and can be easily fabricated, this membrane can be potentially used for numerous practical applications, such as filter membranes with adjustable pores, membrane-based sensors, membrane-based actuators, and multifunctional membranes.

1. Introduction

The programmed movements of stimuli-responsive hydrogels have attracted considerable attention because of their abundant functions and wide range of engineering applications.[1–4] Various stimuli-responsive hydrogels have been patterned through photolithography. For example, the swelling of a surface-attached hydrogel with periodic holes creates compressive stress in the hydrogel and occurs various types of surface instabilities, such as buckling, wrinkling, or creasing.[5–11] The preformed patterns on a hydrogel also induce the reversible buckling or self-folding origami.[12–15] In addition, bilayer polymers composed of differentially swelling hydrogels can be bent or curved.[16–19] The design and control of these responsive hydrogel structures are crucial for practical applications.[20]

As an innovative application that utilizes a stimuli-responsive hydrogel, a stomata-inspired membrane (SIM) with temperature-controlled pore sizes is proposed in this study (**Figure 1**A-b). Stomata are tiny pores distributed on the leaf surface (Figure 1A-a). A pair of guard cells open and close the stomata, which function as multisensory turgor-operative valves to exchange gases between a plant and its environment.[21] Biomimetic technologies, such as evaporative pumps and artificial leaves, have been developed based on the functional features of plant leaves.[22–24] Thus far, the advantageous features of stimuli-responsive opening or closing of stoma in a unique hydraulic valve have not been simulated.

In this study, we demonstrate a novel approach to mimic the gating function of stomata by using a temperature-responsive hydrogel. A simple, cost-effective, and high-throughput photolithographic method was employed to pattern a large surface area in a controlled manner.[25–27] In contrast to previous works that fabricated hydrogel actuators which were mostly made with bilayers of different materials,[18,19] the present study used a single material to synthesize an actuating membrane through the polymerization-induced diffusion on the microscale surface of the polymerizing media. In this particular case, monomers and free radicals were diffused to opposite directions, depending on the chemical potential gradient of the polymerizing material. A distinct double part with pores was created within the polymer membrane by single illumination. Each part presents different mechanical functions on the morphological deformation of the membrane. The SIM shrinks to open the pores, similar to stomata, when triggered by a slight temperature change. The use of a single material in double-parted actuators eliminates any risk of delamination. In addition, the morphological configuration of the SIM can be easily controlled by changing the photomask for a specific application. As the SIM utilizes high sensing-to-actuation functions of stimuli-responsive hydrogels and its fabrication is easy, this membrane can be used in numerous practical applications, including filter membranes with adjustable pore sizes, membrane-based sensors, smart valves, and membrane-based actuators.

2. Results and Discussion

The fabricated membranes contain gating pores that respond to simple temperature changes. A UV-curable poly(*N*-isopropylacrylamide) (PNIPAAm) hydrogel was used for

H. Kim, Prof. S. J. Lee
Center for Biofluid and Biomimic Research
Department of Mechanical Engineering
Pohang University of Science and Technology
Pohang 790-784, Republic of Korea
E-mail: sjlee@postech.ac.kr

DOI: 10.1002/adfm.201501445

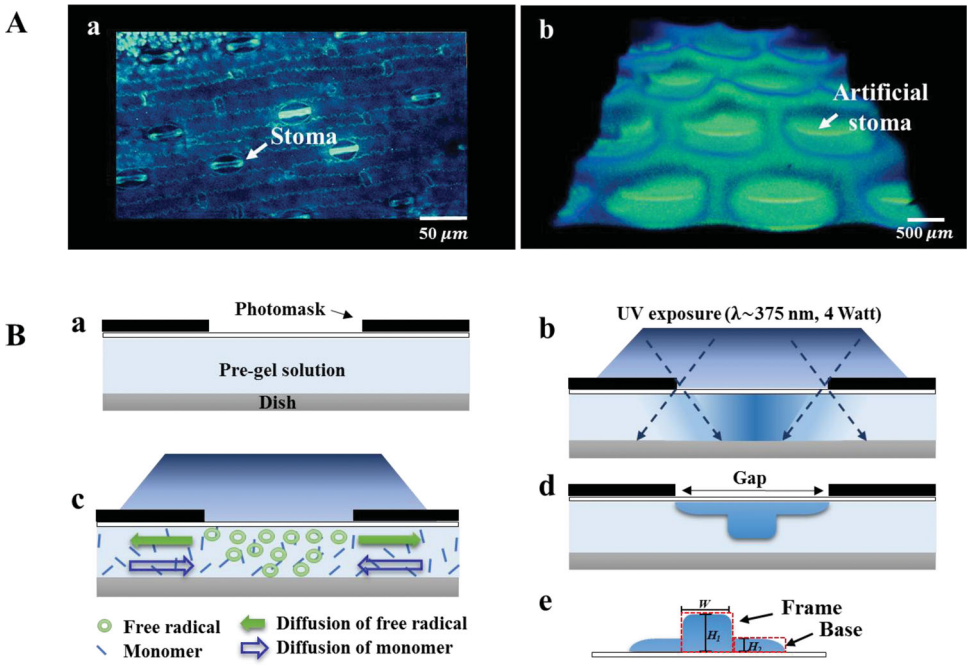

Figure 1. A-a) Surface morphology of a sorghum leaf visualized by a confocal microscopy. A-b) Artificial stomata-inspired membrane (SIM) fabricated with thermally responsive PNIPAAm. B) Schematic of the SIM photopolymerization procedure. B,a) Pre-gel solution is poured between the photomask and a dish. B-b) Pre-gel solution is irradiated by UV light through the transparent photomask. B-c) Monomers and free radicals are diffused in opposite directions, depending on the chemical potential gradient. B-d) During polymerization, the cross-linked PNIPAAm membrane is covalently attached to the photomask substrate. B-e) The relatively thick part is designated the frame, and the thin part is the base.

polymerization-induced diffusion of an irradiated surface at a scale of several hundred micrometers.

2.1. Fabrication of Double-Parted SIMs

A photocrosslinkable pre-gel solution was illuminated with UV light through various photomasks to prepare the photopatterned hydrogel membranes. Optical images were captured from the top of the photomask with an interval of 30 s and are shown in **Figure 2**. The figure demonstrates the UV-polymerization process of the SIM. The dotted circle with 500 μm diameter indicates the mask pattern where UV light are not directly reached the membrane. After 3 min of UV-light exposure, the transparent pre-gel solution is moderately polymerized and an opaque white color appears (Figure 2a). The middle portions between the mask patterns become opaque, and a lattice frame is gradually formed (Figure 2b). Similarly, the remaining regions gradually become opaque as polymerization progressed (Figure 2c,d). After 5 min of UV exposure, most portions of the membrane, except the mask patterns, are filled with the opaque polymer (Figure 2e). The relatively thick part at the middle of the mask pattern is designated as the frame, and the thin part around the frame was named as the base (Figure 1B-e).

Polymerization-induced diffusion was used to transport monomers and free radicals in the polymerizing medium. The diffusion process is driven by the chemical potential gradient of the reactants, and this gradient is affected by several factors, such as reactivity, concentration, diffusion constant, or surface-free energy.[19] In this study, we simplified the driving force for the diffusion process and used the UV light intensity across the illumination region. The site-specific exposure of UV light on the transparent mask pattern initiates polymerization in the middle regions of maximum light intensity. Because the photomask of uniform thickness is highly transparent, the light scattering effect would be negligible. As the light diffraction usually occurs at the edge of the mask pattern, the light intensity is diminished in the region near the mask pattern. Because the light passing through the mask has a Gaussian intensity distribution, the crosslinking starts earlier in the middle region between the mask patterns, where the light intensity is maximum, compared to the edge of the pattern (Figure 2 inset).[8] In the cross-linked area, monomers are rapidly consumed in the polymerization process, resulting in differences in the concentration distribution of monomers.[18] The concentration gradient induces monomers to diffuse from the surrounding area toward the middle of each pattern (Figure 2 inset, empty arrows). The free radicals generated in the UV-irradiated region present higher concentration than that in the unexposed part. These free radicals diffuse from the UV-exposed region toward the unexposed region via the concentration gradient (Figure 2 inset, solid arrows). With these different diffusion mechanisms, a thick frame is formed at the middle of each pattern and a thin base is built around it.

The diffusion of particles is generally expressed by the Fick's second law $\frac{\partial c}{\partial t} = -\frac{\partial}{\partial x} J = \frac{\partial}{\partial x}\left(D\frac{\partial c}{\partial x}\right)$, where J is the flux of particles, D is the diffusion coefficient of particles, c is the particle concentration, and x is the spatial parameter.[18] The concentration distribution of particles obtained using the

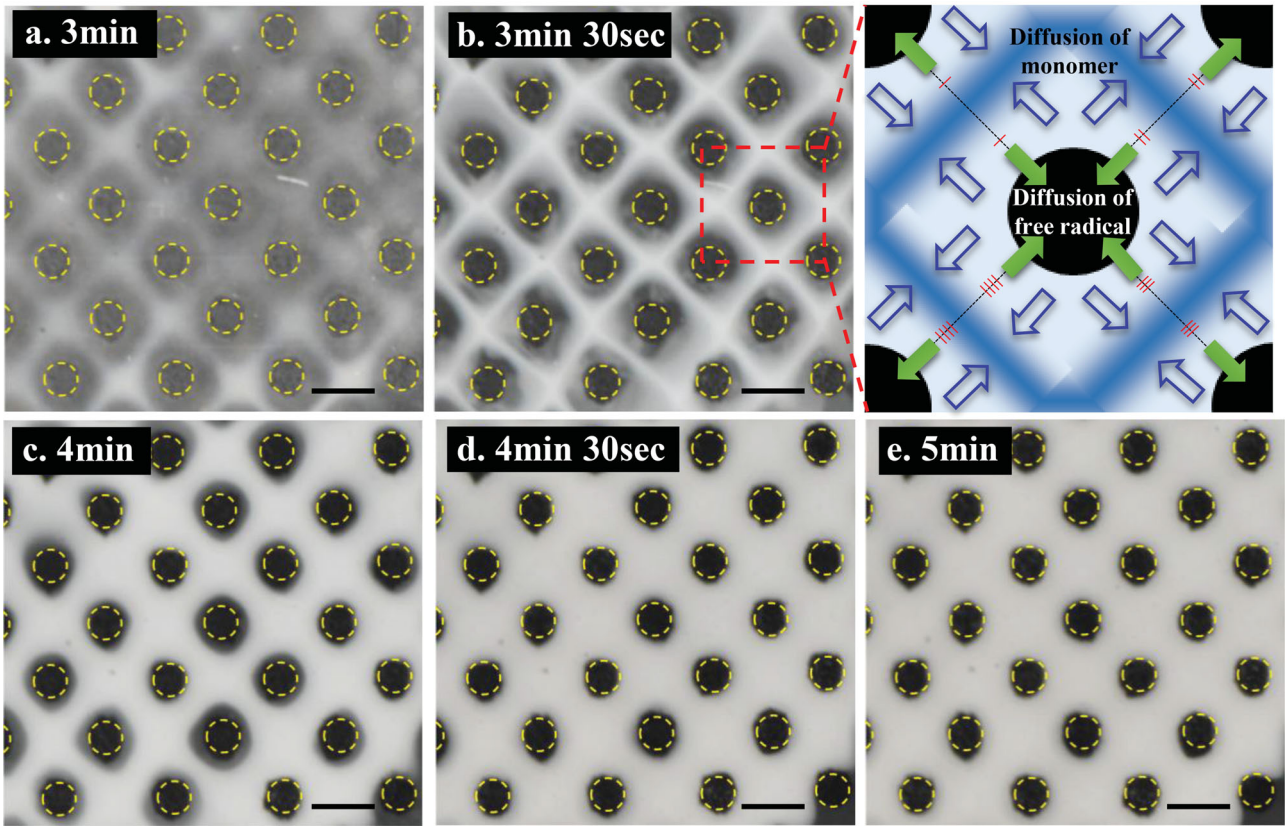

Figure 2. Sequential optical images of the stomata-inspired membrane under UV-polymerization as captured from the top of the photomask with intervals of 30 s. The dotted circles indicate the mask patterns that are not directly reached by UV light. Inset describes the scheme of the polymerization-induced diffusion process to transport monomers and free radicals in the polymerizing medium. Scale bar: 1 mm.

Fick's second law can be expressed as a function of time, diffusion coefficient, distance, and particle concentration at the source. To simplify the solution, we assumed that the polymerization time is fixed and the diffusion coefficient is constant. The initial concentration of photoinitiator in the pre-gel solution and the gap size in the patterns are selected as decisive factors to control the spatial distribution of free radicals.

2.2. Effect of Photoinitiator Concentration

The effect of photoinitiator (PI) concentration on the morphology of the fabricated SIMs was analyzed. Six different pre-gel solutions (PI 1-6) were used to prepare SIMs. These solutions contained identical amounts of the monomer (100 mg) and the crosslinker (1 mg) but different amounts of the photoinitiator (0.5, 0.75, 1, 1.5, 2, and 2.5 mg; Table S1, Supporting Information). **Figure 3**A-a–f shows the optical images of SIMs fabricated with PI 1-6 pre-gel solutions, respectively. These images show the opposite sides of the photomasks after turning them over. The dotted circles in the figure represent the regions of the mask patterns that are not directly reached by UV light. Although each pre-gel solution was illuminated with UV light for 4 min by using the same photomask, the fabricated SIMs exhibit different degrees of polymerization. Overall, as the photoinitiator concentration increases, more monomers are polymerized during the same period of UV exposure. For SIM with PI 1 solution, the thickness of the formed polymers is insufficient to be detected, although polymerization definitely occurred (Figure 3A-a). For the SIM with the PI 2 solution, the gaps between the mask patterns are gradually filled with the polymer (Figure 3A-b). In the case of PI 3 (Figure 3A-c), most spaces between the mask patterns are filled with the polymer. For the SIM with PI 4 solution, even the unexposed regions are covered with the polymer (Figure 3A-d). The regions are severely hidden in the SIMs with PI 5 and 6 (Figure 3A-e,f). In the unexposed regions, polymerization may occur through lateral diffusion of free radicals in the UV-exposed area.[13] A small amount of free radicals may be locally generated because UV light reached the unexposed region through diffraction,[12] and the polymerized thick hydrogel may press itself and cover the unexposed pore regions.

The cross-sections of SIM samples were observed with a confocal microscope. PI 1 solution cannot form a solid membrane, whereas SIM fabricated with PI 2 is insufficiently stiff to be used as a sample for confocal imaging. Figure 3B-a–d presents the cross-sectional images of SIMs fabricated with PI 3-6 solutions, respectively. These figures were photographed at 150 μm below the top of the membranes. SIM with PI 3 clearly presents pores whose size is almost identical to the mask patterns (Figure 3B-a). The pores of SIM with PI 4 demonstrate a waffled shape

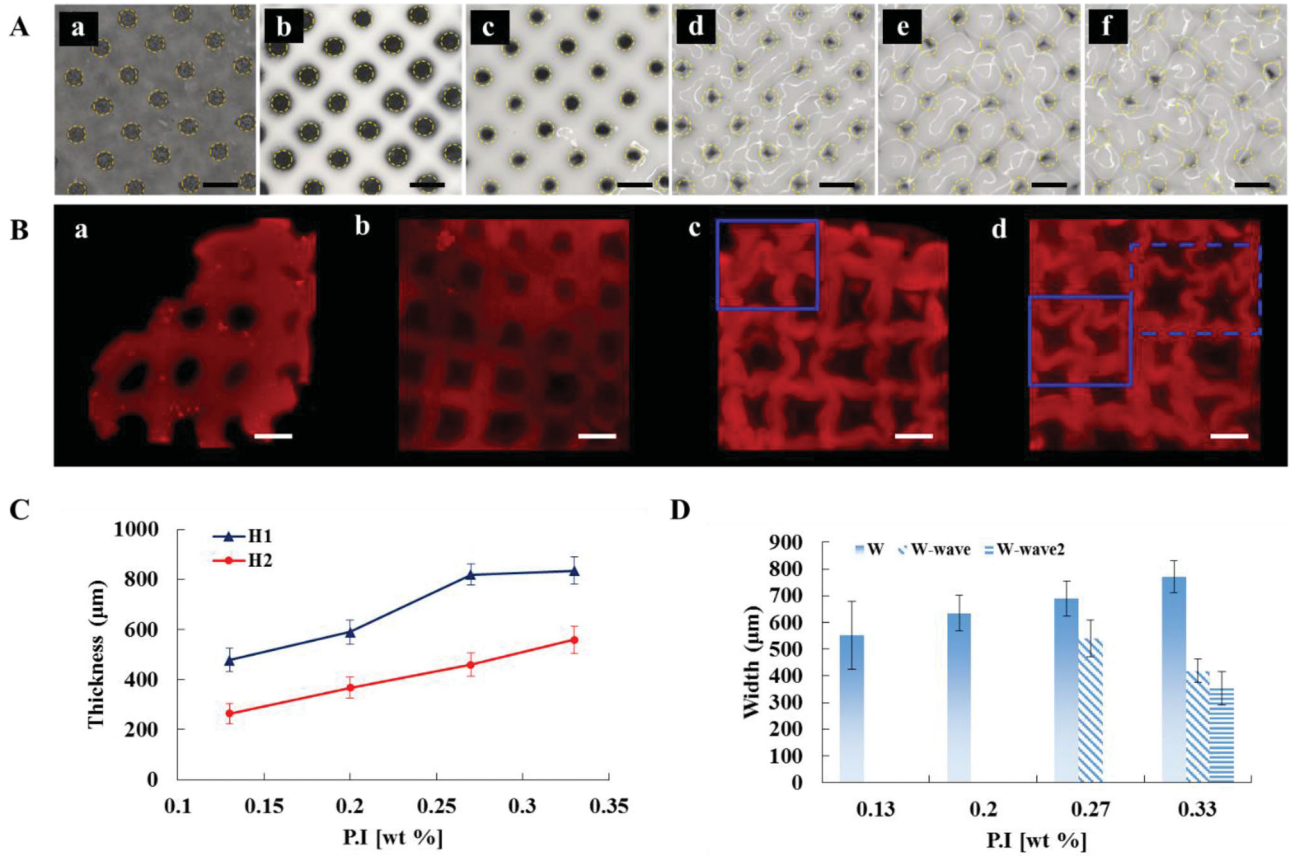

Figure 3. A) Optical images of the fabricated stomata-inspired membranes with PI 1-6 pre-gel solutions, respectively. B) Cross-sectional images of SIMs with PI 3-6 as captured at approximately 150 μm below the top of the membranes. C) Variations in the average thicknesses of the frame (H_1) and base (H_2). D) Comparison of the average widths of the straight line frames (solid bars), the wrinkle frames with one wave (diagonal lines), and the wrinkle frames with more than one wave (horizontal lines). Scale bar: 1 mm.

with straight line frames (Figure 3B-b). For SIM with PI 5, the combined configuration of straight lines and wrinkled frames with a wave appears (inside a line box) (Figure 3B-c). SIM with PI 6 also presents the combined configuration of straight lines and wrinkled frames with more than one wave (Figure 3B-d). The average thicknesses of the frame and base are compared in Figure 3C. As photoinitiator concentration increases, the thicknesses of both almost linearly increase. This trend indicates that the polymerization rate is proportional to photoinitiator concentration, because more photoinitiators generate more free radicals. This result is accordance with the solution of Fick's second law expressed as $c = c_0\left(1-\left(\frac{x}{\sqrt{Dt\pi}}\right)\right)$, where the concentration distribution of free radical (c) is proportional to its initial concentration (c_0). The average width of each frame is depicted in Figure 3D. The average width of the line frames excluding the wrinkled waves increases as PI concentration increases (solid bars). The width of the wrinkled frames with waves is smaller than that of the line frames (diagonal lines). As the number of waves in wrinkle frames increases, the average width decreases (horizontal lines). These results indicate that in the presence of an abundant amount of photoinitiator in the pre-gel solution in the narrow regions, polymerization selectively produces a straight thick frame or a wavy thin frame.

2.3. Effect of Gap Size

The effect of the gap size in the mask patterns on the morphological structures of fabricated SIMs was investigated with three different photomasks of different gap sizes. The optical images of SIMs fabricated with mask patterns with different gap sizes are shown in **Figure 4**A. Images in the first line show the optical images captured from the opposite side of the photomasks. The dotted circles in the figure indicate the regions that are not directly reached by UV light. The gap distances (α,β) between the adjacent patterns in the three different photomasks are (500, 880), (700, 1150), and (900, 1630) μm. Although PI 3 solution was equally irradiated for 4 min for the three photomasks, the fabricated SIMs exhibit different polymerization patterns (Figure 4A-a–c). All three SIMs present straight line frames. The width between the straight line patterns gradually increases as the gap size in the mask patterns increases (Figure 4B-a–c). The average thicknesses of the frame and base are compared in Figure 4C. The thicknesses of both increase as the gap size in the mask patterns increases. The average width in the frame also increases with increasing gap size (Figure 4D). The ratio of the width to the gap of the frame (width/gap size × 100) decreases from 63% to 50% as the gap size increases (Figure 4D). These results indicate that polymerization is more

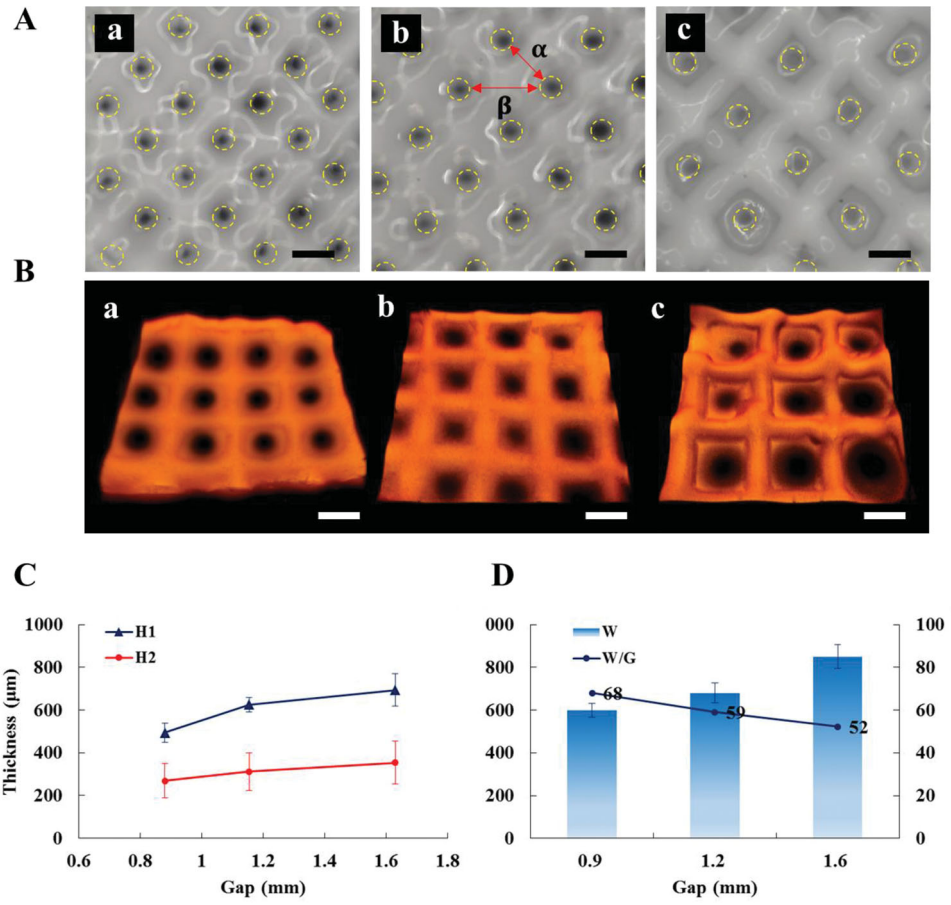

Figure 4. A) Optical images of stomata-inspired membranes (SIM) fabricated with photomasks of various gap sizes between the mask patterns. The gap distances (α, β) between the mask patterns of three different photomasks are a) (500, 880) μm, b) (700, 1150) μm, and c) (900,1630) μm. B) The corresponding 3D images of SIMs in (a) to (c). C) Variations in the average thicknesses of the frame and base. D) Average widths of the frame and the ratios of the width to the gap (width/gap size × 100) for three different gaps. Scale bar: 1 mm

pronounced in wide-exposed area as induced by the large gap size in the mask patterns. By conducting scaling analysis on the Fick's first law, the diffusive flux (J) can be simply expressed as $J = D\frac{\partial c}{\partial x} \sim \frac{C_r}{G}$, where C_r is the characteristic concentration of free radical and G is the characteristic gap size. As the gap size increases, the diffusive flux of free radical decreases, and more free radicals are remained in the gap area and then more polymerization is initiated.

2.4. Thermal Response of SIMs

To analyze the deformational features of SIMs in response to temperature changes, we fabricated an SIM with a honeycomb shape (**Figure 5**A-a). A hexagonal geometry has been reported as the most efficient structure for absorbing stress induced by structural deformation.[29] For the hexagonal geometry, the base of the fabricated membrane presents the maximum surface area and the minimum length of the frame. To examine the structural variation of each part according to temperature change, we increased the temperature of the freely suspended honeycomb-shaped SIM higher than the lower critical solution temperature (LCST) of PNIPAAm (32 °C). Figure 5A-b,c shows the initial and final states of the honeycomb-shaped SIM, respectively. The water extruded from SIM causes the PNIPAAm network to entirely shrink on the whole. The shrinkage of the membrane occurs at the LCST of PNIPAAm. On average, the surface area shrinks by up to 80.4% of the initial area and the average area of pores decreases by approximately 70.2% of the initial area. The temporal variations in the linear strain values of the frame and base along the tangential and radial directions are compared in Figure 5B. As SIM was heated, all the strain values negatively increased. This means the SIM shrinks in all directions. The strain of the base along the radial direction maintains the highest values, followed by the base along the tangential direction and the frame along the radial direction. The frame along the tangential direction presents the lowest strain values.

For the case of freely suspended membranes, swelling is isotropic and identical in all directions. The linear swelling ratio α_x is evaluated by the equation $\alpha_x = \frac{l_{x,s}}{l_{x,d}}$, where $l_{x,s}$ is the length in the arbitrary direction x of the membrane

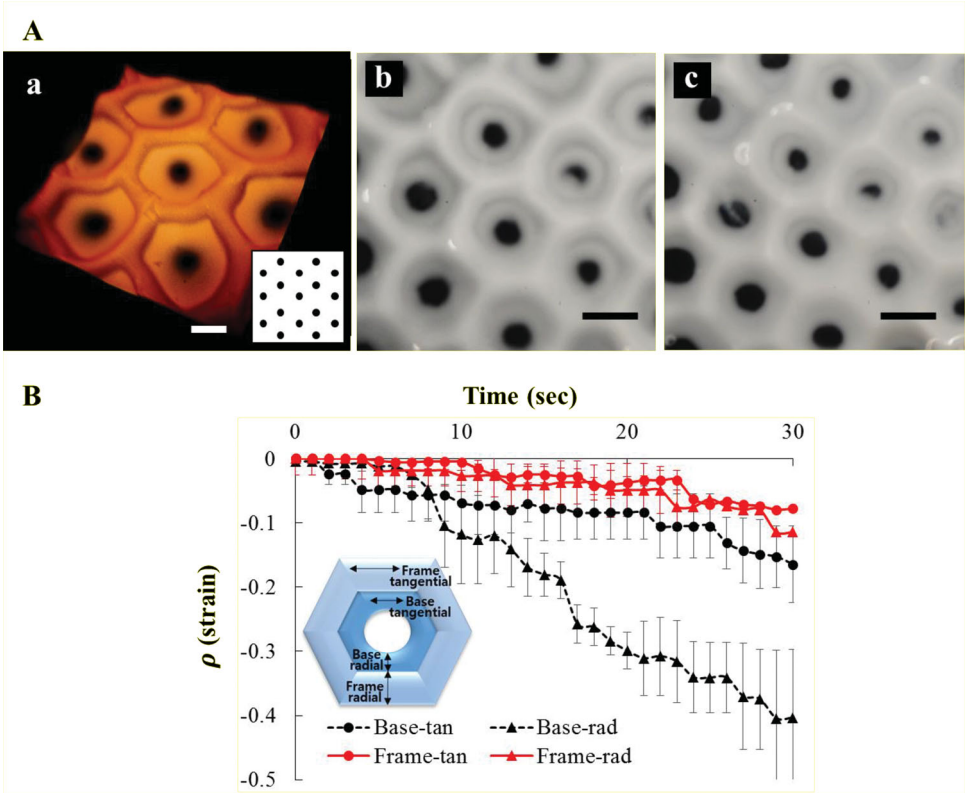

Figure 5. Temporal variation of the 3D structure and linear strain of the freely suspended honeycomb-shaped stomata-inspired membrane (SIM) when the heated temperature is higher than the LCST of the PNIPAAm. A- a) 3D structure of the honeycomb-shaped SIM fabricated using the dotted photomask (inset). b) Optical image of the initial state of the honeycomb SIM. c) Optical image of the final state of the honeycomb-shaped SIM after heating. B) Temporal variation in the linear strain values of the frame and base along the tangential and radial directions. Scale bar: 1 mm.

at the swollen state, whereas $l_{x,d}$ is the length in the same direction at dry condition.[19,28] During shrinking, the linear strain can be expressed as a function of the linear swelling ratio $\rho_{x,f} = \frac{l_{x,f} - l_{x,o}}{l_{x,o}} = \frac{l_{x,d}}{l_{x,s}} - 1 = \frac{1}{\alpha_x} - 1$. Hence, the relationship of $\alpha_x = \frac{1}{\rho_{x,f} + 1}$ is satisfied. After 30 s of heating, the maximum strain values of the frame in the tangential and radial directions are −0.08 and −0.01, respectively. The corresponding linear swelling ratios derived from the above relationship are 1.09 and 1.01, respectively. The linear strain values of the base in the tangential and radial directions are −0.16 and −0.4, and the corresponding linear swelling ratios are 1.19 and 1.67, respectively. Comparison of the linear swelling ratios shows that the base in the radial direction exhibits the largest linear swelling and predominantly determines the morphological configuration of the membrane (**Table 1**). In addition, the swelling ratios of the base in both directions are higher than those of the frame. As the crosslinker in the pre-gel solution is consumed during the polymerization, it is diffused toward the middle of the exposed area. Then the concentration of the crosslinker in the frame becomes higher than that of the base. The slightly cross-linked polymer in the base represents a higher degree of swelling ratio, compared to the highly cross-linked polymer in the frame.[30,31] These results imply that polymer density in the base is smaller than that in the frame.[32,33] Actually, the measured density of the base (5.95×10^{-7} μg/μm^3 (±0.08)) is almost three times smaller than that of the frame (1.79×10^{-6} μg/μm^3 (± 0.2)). The experimental results are statistically significant ($p < 0.01$).

For the case of constrained deformation, only the pores are deformed as evidenced by the anchored edge of the honeycomb-shaped SIM to the glass substrate. **Figure 6**A-a,b shows the initial and final equilibrium states, respectively, of SIM after deformation. During heating of SIM, the shrinkage of the membrane causes stress and this shrinkage-induced stress considerably increases the size of circular pores. The average pore surface area increases by 441% of the original pore area, but the surface area of the membrane does not change. The temporal variations in the linear strain values of the frame and base along the tangential and radial directions are depicted in Figure 6B. The linear strain values in the radial direction of the frame and base become more negative when SIM was heated. This trend indicates that the membrane shrinks along the radial direction. By contrast, the linear strains in the tangential direction of both demonstrate positive values, which increase with time. This increase implies that the membrane is stretched in the tangential direction. After 30 s of constrained deformation, the maximum strain values of the frame in the tangential and radial directions are 0.03 and −0.13 and the corresponding linear swelling ratios are 0.97 and 1.15, respectively (Table 1). As the swelling ratios of the frame are almost 1, the frame is slightly deformed but maintains the stability of the whole structure. The maximum linear strain values in the tangential

Table 1. Comparison of the linear strain, swelling ratio, and expansion ratio of pore radius of the SIMs.

Free deformation						
		Tangential	Radial		Tangential	Radial
Maximum linear strain (ρ_x)	Frame	–0.08	–0.01	Base	–0.16	–0.4
Linear swelling ratio (α_x)		1.09	1.01		1.19	1.67
Constraint deformation						
		Tangential	Radial		Tangential	Radial
Maximum linear strain (ρ_x)	Frame	0.03	–0.13	Base	0.48	–0.33
Linear swelling ratio (α_x)		0.97	1.15		0.67	1.49
Expansion ratio of pore radius						
Honeycomb	$r_{avg} = 1.37$					
Monocot inspired SIM	$r_{avg} = 2.9, r_{90°} = 0.64, r_{270°} = 0.33$					
Dicot inspired SIM	Horizontal (1 mm)		$r_{avg} = 2.3, r_{90°} = 0.67, r_{270°} = 0.20$			
	Vertical (1.5 mm)		$r_{avg} = 1.94, r_{0°} = 0.07, r_{180°} = 0.12$			

and radial directions of the base are 0.48 and –0.33, and the corresponding linear swelling ratios are 0.67 and 1.49, respectively. Therefore, the base is stretched in the tangential direction and shrinks in the radial direction with increasing temperature. This motile mechanism predominantly determines the morphological shape of the pores. The radius expansion ratios ($r\alpha$) of pores with an angle interval of 45° are presented in Figure 6C. The radius expansion ratios along the eight axes exhibit similar values, with an average value of 1.37. The gray region in the graph indicates the standard deviation. This result demonstrates that the pores of the honeycomb-shaped SIM can uniformly open and close their apertures in all directions.

2.5. Various Configurations of SIMs

To construct the artificial stomata of a monocot leaf, which are lined up in parallel, a photomask of horizontal slit patterns of 1 mm in length was used for photopolymerization (**Figure 7**A inset). The frame of the resultant SIM presents a diamond shape, and the base exhibits slit-like horizontal pores (Figure 7A-a,b). When the monocot-inspired SIM was heated, the slits open and expand to an almost elliptical configuration (Figure 7A-c). The radius expansion ratios along the 90° axis ($r_{90°} = 0.64$) and the 270° axis ($r_{270°} = 0.33$) are nearly zero, whereas the average of radius expansion ratios along the other directions is almost 2.9 (Figure 7A-d). This trend is attributed to the fact that both ends of the slits are constrained, but the slits are comparably free to deform along the other directions. The average radius expansion ratio of the monocot-inspired SIM (2.9) is twice higher than that of the honeycomb-shaped SIM (1.37). This difference implies that the slit pores of the monocot-inspired SIM expand to a wider degree than the circular pores of the honeycomb-shaped SIM (Table 1).

To simulate the randomly distributed stomata of a dicot leaf, a patterned photomask mixed with a horizontal slit of 1 mm and a vertical slit of 1.5 mm in length was used for photopolymerization (Figure 7B inset). The resultant dicot-inspired SIM demonstrates a hexagon-shaped frame, whereas the base contains a combination of slit-like horizontal and vertical pores (Figure 7B-a,b). After the edge of the dicot-inspired SIM was constrained and heated, the slits open and expand to an almost elliptical configuration (Figure 7B-c). In the horizontal slits, the radius expansion ratios of $r_{90°}(=0.67)$ and $r_{270°}(=0.20)$ are nearly zero, whereas the average value along the other directions is approximately 2.3 (Figure 7B-d, solid line). For vertical slits, $r_{0°}(=0.07)$ and $r_{180°}(=0.12)$ are nearly zero and the average values along the other directions is approximately 1.94 (Figure 7B-d, dashed line). As inferred from the higher average radius expansion ratio of the horizontal slits (2.3) than that of the vertical slits (1.94), shorter slits expand wider than longer slits.

The constrained shrinkage of SIM causes anisotropic in-plane compressive and tensile stresses. A schematic diagram describing the deformation of one slit pore of SIM is presented in **Figure 8**. Assuming that shrinkage in the z-direction does not significantly affect the the change of lateral pore area, the gating of the pore can be considered as a 2D problem. Given that the edge of the SIM is constrained, the SIM deforms only along the x-direction. The shearing strain is defined as change in the angle α. Therefore, the rate of shearing strain can be expressed as $\delta\alpha = \frac{\partial u_x}{\partial y} \cdot \delta t$, where u_x is the rate of deformation in the x-direction. The shear strain of shrinkage is then expressed as $\alpha = \frac{\partial u_x}{\partial y}$. By conducting scaling analysis, the relationship of $\alpha \sim \frac{R/\tau}{L}$ is derived, here R and L are the characteristic width and length of the pore, respectively, and τ is the characteristic time of pore gating. Therefore, the total deformation (D) can be represented as $D = \alpha \times \tau \approx \frac{R}{L}$ (Equation 2). This relation is confirmed by the radius expansion ratios of the horizontal slits to the vertical slits (Figure 6B-d). This relation implies that the aperture of an open pore is proportional to the ratio of the width and length of the pore. On average, the R/L ratio of the vertical slits is 0.34 with a standard deviation of 0.06, whereas that for the horizontal slits is 0.42 with a standard deviation of

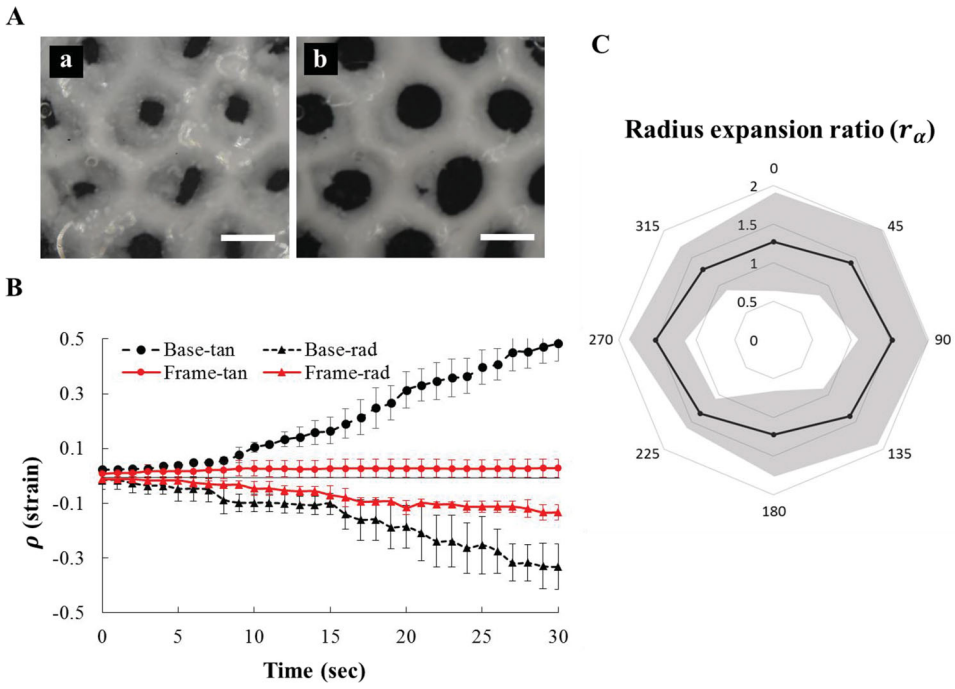

Figure 6. Optical images, linear strain values, and radius expansion ratios of the constrained honeycomb-shaped stomata-inspired membrane (SIM) when the heated temperature is higher than the LCST of PNIPAAm. A) Optical images of the initial state a) and the final state after heating b) the SIM. B) Temporal variation in the linear strain values of the frame and base along the tangential and radial directions. C) Angular variation of the radius expansion ratios (r_α) of the pores with intervals of 45°. The solid line represents the average values of r_α, and the gray region indicates the standard deviation. Scale bar: 1 mm.

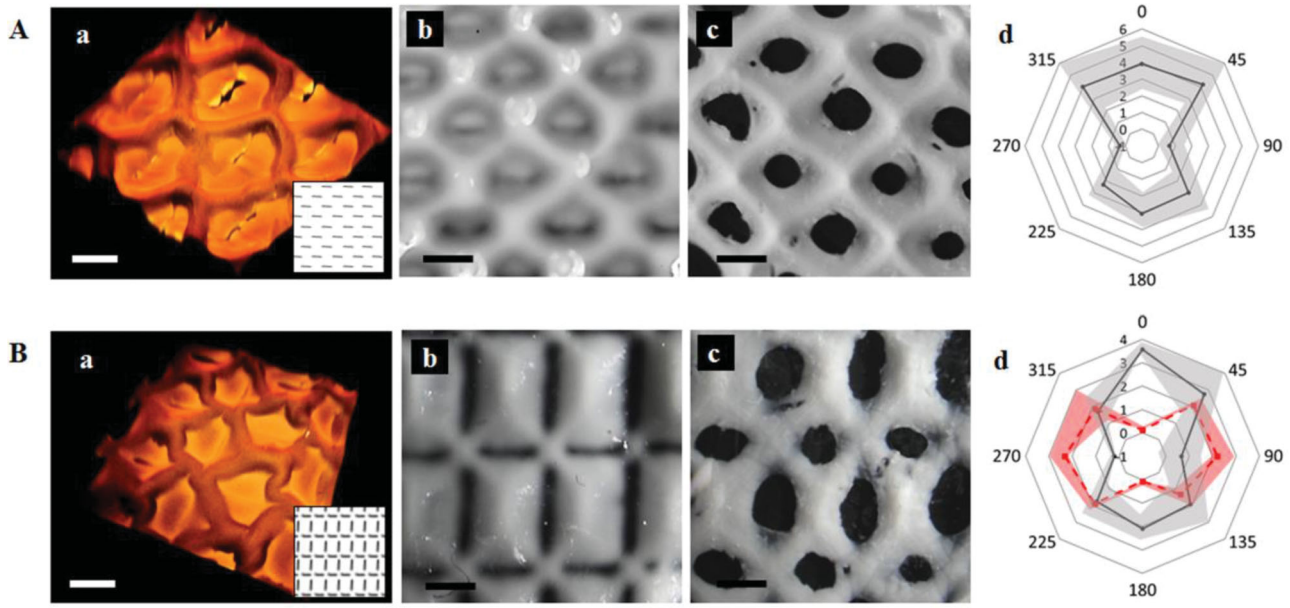

Figure 7. Deformation of stomata-inspired membrane (SIM) with slit-like pores. A-a) Confocal image of the resultant monocot SIM. Inspired by monocot leaf stomata, the horizontal slit patterns of the photomask is used for photopolymerization (inset). b) Optical image of the initial state of the monocot SIM. c) When the SIM is heated, the slits open and expand to almost elliptical shapes. d) Angular variation in the radius expansion ratio (r_α) of the slit with an interval of 45°. Solid line graph represents the average values of r_α, and the gray region indicates the standard deviation. B- a) Confocal image of the resultant dicot SIM. Inspired by dicot leaf stomata, horizontal and vertical slit patterns are combined in the photomask (inset). b) Optical image of the initial state of dicot SIM. c) Slits open and expand to almost elliptical shapes through heating. d) Angular variation of the radius expansion ratio (r_α) of the slit with an interval of 45°. The solid line graph represents the average values of the r_α horizontal slits, and the dashed line graph indicates the values of vertical slits. Scale bar: 1 mm.

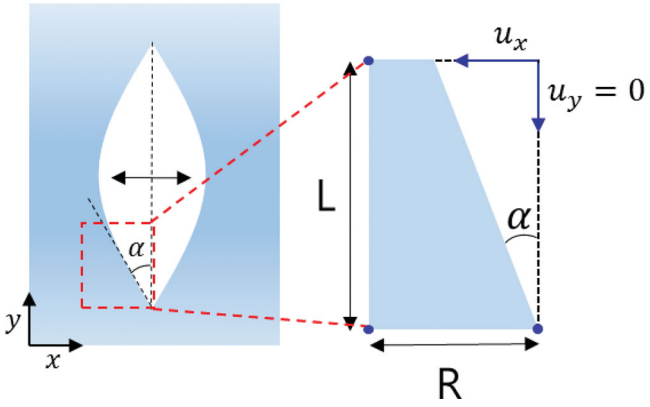

Figure 8. Schematic of the deformation of a slit pore in stomata-inspired membrane (SIM). The SIM only deforms along the *x*-direction because of the constrained edge. The engineering shear strain is defined as change in the angle α.

0.06. As expected from the above relation, the horizontal slits, whose R/L ratio is much larger than that of vertical slits have larger radius expansion ratios, compared to that of vertical slits.

3. Conclusion

In this study, we fabricated an innovative SIM by using temperature-responsive PNIPAAm. During fabrication of photopolymerization-based patterns, polymerization-induced diffusion was effectively utilized on the macroscale surface. The diffusion induced by chemical potential gradient causes monomers in the pre-gel solution to accumulate in the region illuminated with high-intensity UV light, thereby accelerating polymerization. Free radicals are also dispersed to the unexposed area, and polymerization is decelerated at the edge of the mask patterns. Consequently, a double-parted polymer membrane with controllable pores was fabricated after single exposure to UV light and each part exhibits different mechanical functions. The thick part of less deformable material supports the whole structure. Another thin part of largely deformable material dominantly regulates pore shape. A comparison of the deformational features of SIMs with different shapes reveals that the slit pores of monocot-inspired SIM exhibit the maximum radius deformation.

Stomata are well-organized multisensory turgor operative valves. Similar to stomatal movement regulated by water uptake or release of guard cells,[21] the fabricated SIMs can regulate the shape of pores by swelling or shrinking a thermally responsive hydrogel. The less deformable frame is analogous to the subsidiary cells that surround and support the guard cells. The base, which dominantly determines the shape of pores in the SIM, has a role similar to that of the guard cells of stomata. The developed SIM is an intelligent membrane that can sense and react to environmental changes. In addition, the temperature-responsive deformation of the SIM is reversible under wet condition (Figure S4, Supporting Information). Moreover, the morphological configuration of the SIM can be easily controlled by selecting a suitable photomask for a specific application. Considering the sensors to actuators fabricated by the simple and controllable photopolymerization-based patterning, stimuli-responsive SIM can be potentially applied to numerous engineering applications in the future.

4. Experimental Section

Synthesis of SIM: Photocrosslinkable PNIPAAm was synthesized via the free-radical polymerization method to fabricate SIM. A pre-gel solution was prepared by dissolving 100 mg of *N*-isopropylacrylamide monomer (NIPAAm; Sigma Aldrich) in 0.7 mL of deionized water. Subsequently, 1 mg of *N*,*N*′-methylenebisacrylamide (MBAm; Sigma Aldrich) and 1 mg of 2-hydroxy-1-[4-(hydroxyethoxy)phenyl]-2-methyl-1-propanone (Irgacure 2959; Sigma Aldrich) were added to the monomer solution as a crosslinker and a photoinitiator, respectively (Figure S1, Supporting Information). Various patterns were designed and printed on transparent photomasks. The pre-gel solution was poured into a space between the photomask and a dish to synthesize PNIPAAm (Figure 1B-a). The solution was covered with the photomask and then irradiated for 4 min with UV light (VIRVER Lourmat-4.L, France; λ = 365 nm, 4 W) (Figure 1B-b). Free radicals were generated in the illuminated regions, and polymerization was then initiated. The monomers and free radicals diffused in opposite directions, depending on the chemical potential gradient in the polymerizing medium (Figure 1B-c). During the polymerization process, the monomers were cross-linked into a network and the cross-linked PNIPAAm was covalently attached to the photomask substrate (Figure 1B-d).[34] The relatively thick part of the double-parted SIM was designated as the frame, and the thin part was the base (Figure 1B-e). The SIM was carefully peeled off from the photomask and dipped in deionized water. In the meantime, the SIM was fully hydrated and excess reactants were dissolved out. To measure the densities of the frame and base, each part was mechanically separated. Their mass was measured with a microbalance (±0.5 μg), and its volume was estimated from the 3D tomography data with a spatial resolution of 2 μm. The density of the polymer was calculated by dividing the measured mass with the estimated volume (μg/μm^3).

Morphological Structure of SIM: The surface morphologies of the fabricated SIMs were observed with a stereoscope (Stemi 2000c; Zeiss, Germany) attached to a digital camera (NIKON D700). The samples were stained with rhodamine-B solution and imaged using a Leica-SP5 confocal microscope with a 5× objective lens to visualize the 3D morphological structures of the SIMs. The captured images were post-processed with the commercial Leica software. The 3D configuration of each SIM was reconstructed using the Amira software (Visualization Science Group). The thicknesses of the frame (H_1) and base (H_2) of the SIMs were measured from the cross-sectional images (Figure S2A, Supporting Information). The frame and base can be clearly distinguished based on the inflection points of light intensity across the membrane (Figure S2B, Supporting Information). The width of the frame (W) is defined as the distance from one inflection to another inflection point.

Measurement of Structural Changes: The LCST of PNIPAAm is approximately 32 °C. At temperatures higher than the LCST, the material shrinks and the surface becomes hydrophobic with a contact angle of 90.1° ± 1.1°. At temperatures lower than the LCST, PNIPAAm swells and presents a hydrophilic surface with a contact angle of 71.1° ± 6.3° (Figure S3, Supporting Information).[35,36]We heated the fully hydrated SIM at a rate of 3 °C min^{-1} using a Peltier chip to increase the temperature in the range from 30 °C to 36 °C. For free deformation, the SIM was freely placed on a glass surface and heated. For constrained deformation, the edge of the membrane was anchored to the glass with adhesive glue and then heated in the same manner. All experiments were conducted at room temperature (25 °C). Images of the deformed SIM samples were consecutively captured at a frame rate of 3 fps by using a digital camera (NIKON D700) attached to a stereoscope. Linear strain is defined by the equation: $\rho_x(t) = \frac{l_x(t) - l_x(t=0)}{l_x(t=0)}$, where $\rho_x(t)$ is the linear strain along the *x* direction at time *t* and l_x represents the *x*-directional length of the membrane, which was calculated from the length measurement data.

The radius expansion ratio r_α is defined as $r_\alpha = \frac{r_{\alpha,f}-r_{\alpha,i}}{r_{\alpha,i}}$, where r_α is the radius expansion ratio along the α° axis and $r_{\alpha,i}$ and $r_{\alpha,f}$ represent the initial and final radii along the α° axis, respectively. The radius expansion ratios of the SIM pores were measured at an angle interval of $\alpha = 45^\circ$.

Supporting Information

Supporting Information is available from the Wiley Online Library or from the author.

Acknowledgements

This study was supported by the National Research Foundation of Korea (NRF) and funded by the Korean government (MSIP) (Grant No. 2008-0061991).

Received: April 10, 2015
Revised: May 9, 2015
Published online: June 13, 2015

[1] D. J. Beebe, J. S. Moore, J. M. Bauer, Q. Yu, R. H. Liu, C. Devadoss, B. H. Jo, *Nature* **2000**, *404*, 588.
[2] A. Lendlein, H. Jiang, O. Jünger, R. Langer, *Nature* **2005**, *434*, 879.
[3] R. Geryak, V. V. Tsukruk, *Soft Matter* **2014**, *10*, 1246.
[4] L. Ionov, *Mater. Today* **2014**, *17*, 494.
[5] Y. Zhang, E. A. Matsumoto, A. Peter, P. C. Lin, R. D. Kamien, S. Yang, *Nano Lett.* **2008**, *8*, 1192.
[6] G. Wu, Y. Xia, S. Yang, *Soft Matter* **2014**, *10*, 1392.
[7] V. Trujillo, J. Kim, R. C. Hayward, *Soft Matter* **2008**, *4*, 564.
[8] M. Guvendiren, J. A. Burdick, S. Yang, *Soft Matter* **2010**, *6*, 5795.
[9] Z. Wu, N. Bouklas, R. Huang, *Int. J. Solids Struct.* **2013**, *50*, 578.
[10] S. Singamaneni, V. V. Tsukruk, *Soft Matter* **2010**, *6*, 5681.
[11] D. Chandra, A. J. Crosby, *Adv. Mater.* **2011**, *23*, 3441.
[12] J. Bae, J. H. Na, C. D. Santangelo, R. C. Hayward, *Polymer* **2014**, *55*, 5908.
[13] Q. Du, Y. Guan, J. X. Zhu, Y. Zhang, *Soft Matter* **2015**, *11*, 10.
[14] J. H. Na, A. A. Evans, J. Bae, M. C. Chiappelli, C. D. Santangelo, R. J. Lang, T. C. Hull, R. C. Hayward, *Adv. Mater.* **2015**, *27*, 79.
[15] C. Yoon, R. Xiao, J. Park, J. Cha, T. D. Nguyen, D. H. Gracias, *Smart Mater. Struct.* **2014**, *23*, 094008.
[16] D. H. Gracias, *Curr. Opin. Chem. Eng.* **2013**, *2*, 112.
[17] X. Z. Zhibing Hu, Yong Li, *Science* **1995**, *269*, 28.
[18] C. M. Leewis, A. M. De Jong, L. J. Van IJzendoorn, D. J. Broer, *J. Appl. Phys.* **2004**, *95*, 4125.
[19] D. Liu, C. W. M. Bastiaansen, J. M. J. d. Toonder, D. J. Broer, *Soft Matter* **2013**, *9*, 588.
[20] A. Sidorenko, T. Krupenkin, A. Taylor, P. Fratzl, J. Aizenberg, *Science* **2007**, *315*, 487.
[21] C. Willmer, M. Fricker, *Stomata*, Chapman & Hall, London **1996**.
[22] T. D. Wheeler, A. D. Stroock, *Nature* **2008**, *455*, 208.
[23] J. M. Li, C. Liu, Z. Xu, K. P. Zhang, X. Ke, L. D. Wang, *PloS One* **2012**, *7*, e50320.
[24] V. Namasivayam, R. G. Larson, D. T. Burke, M. A. Burns, *J. Micromech. Microeng.* **2003**, *13*, 261.
[25] M. Guvendiren, S. Yang, J. A. Burdick, *Adv. Funct. Mater.* **2009**, *19*, 3038.
[26] M. Guvendiren, J. A. Burdick, S. Yang, *Soft Matter* **2010**, *6*, 2044.
[27] M. Jamal, A. M. Zarafshar, D. H. Gracias, *Nat. Commun.* **2011**, *2*, 527.
[28] D. Liu, C. W. Bastiaansen, J. M. Den Toonder, D. J. Broer, *Langmuir* **2013**, *29*, 5622.
[29] V. Deshpande, N. Fleck, *J. Mech. Phys. Sol.* **2003**, *51*, 187.
[30] R. Singhal, R. S. Tomar, A. Nagpal, *Int. J. Plast. Technol.* **2009**, *13*, 22.
[31] R. da Silva, M. G. de Oliveira, *Polymer* **2007**, *48*, 4114.
[32] G. M. Eichenbaum, P. F. Kiser, A. V. Dobrynin, S. A. Simon, D. Needham, *Macromolecules* **1999**, *32*, 4867.
[33] H. Inomata, N. Wada, Y. Yagi, S. Goto, S. Saito, *Polymer* **1995**, *36*, 875.
[34] J. Yoon, J. Kim, R. C. Hayward, *Soft Matter* **2010**, *6*, 5807.
[35] M. A. C. Stuart, W. T. Huck, J. Genzer, M. Müller, C. Ober, M. Stamm, G. B. Sukhorukov, I. Szleifer, V. V. Tsukruk, M. Urban, *Nat. Mater.* **2010**, *9*, 101.
[36] H. Tekin, J. G. Sanchez, T. Tsinman, R. Langer, A. Khademhosseini, *AIChE J.* **2011**, *57*, 3249.